Dynamics of the Ionic Space-Charge Electret State in CaF_2†

Ervin B. Podgoršak and P. R. Moran
Medical Physics Laboratories, Departments of Physics and Radiology, University of Wisconsin, Madison, Wisconsin 53706
(Received 19 March 1973)

The space-charge electret state is strongly correlated with the bulk ionic conduction in CaF_2. Its thermogram is a narrow symmetric peak with a characteristic depolarization temperature which varies around 100 °C depending on logarithmically on the impurity doping concentration. The electret-state polarization-depolarization dynamics show dominant bilinear behavior with a simple thermally activated rate function with a single activation energy. The equilibrium electret polarization is first directly proportional to the polarizing voltage and then for voltages greather than about 250 V follows a $V^{1/2}$ dependence. A typical charge release for a polarizing voltage of 1000 V is 0.05×10^{-6} C cm^{-2} independent of both the sample thickness and impurity concentration.

INTRODUCTION

This paper reports investigation of a strong high-temperature thermoelectret state in relatively high-purity calcium fluoride. In contrast to most other strong electrets, this system appears to be dominated by a singly characterized mechanism. The resulting behavior is sufficiently simple to allow unambiguous identification of ionic conductivity charge transport as the mechanism forming this space-charge electret. For the first time, to our knowledge, the polarization-depolarization dynamics of a space-charge electret can be very well approximated by a single simple expression. For measurements spanning at least a factor of 10^3 variation in polarizing voltage, the electret polarization σ follows the second-order kinetics equation

$$d\sigma/dt = -\gamma(T)(\sigma^2 - \sigma_{eq}^2). \tag{1}$$

In Eq. (1), σ_{eq} is the equilibrium polarization at a polarizing voltage V. We find, for V less than about 250 V, a linear relation:

$$\sigma_{eq} = c_e V. \tag{2}$$

The electret specific capacitance c_e is extremely large (~ 100 pF cm^{-2}), measured in a geometry where the ordinary geometrical capacitance, for comparison, is about 1 pF cm^{-2}.

The second-order rate parameter $\gamma(T)$ is thermally activated;

$$\gamma(T) = \gamma_0 e^{-H/kT}. \tag{3}$$

The preexponential factor γ_0 is empirically found to depend in a simple manner upon the polarizing conditions initially applied to establish the electret state. Not only is the experimentally determined activation energy, H in Eq. (3), identical with that governing the material's bulk ionic conductivity, but the observed relation between $\gamma(T)$ and ionic conductivity is even more extensive. If we represent the polarizing electric field by $\langle E \rangle$, then the product $\sigma_{eq}^2 \gamma(T) \langle E \rangle^{-1}$, which we call the characteristic admitivity, i.e., (reactance cm^2)$^{-1}$, appears under all experimental conditions to be exactly numerically equal to the measured ionic conductivity.

To describe our work further, some background is appropriate. It has long been known that practically any dielectric will, to some degree, form an electret state if subjected to appropriate procedures. An excellent descriptive and qualitative review of the electret behavior has been given by Gross,[1] and more technical reviews by Perlman,[2] Gross,[3] and Mascarenhas.[4] Since the discovery of the electret state (Eguchi,[5] 1925) much experimental work has been undertaken in materials[6–8] ranging from ionic crystals to thin films of polymers. There has been, to our best knowledge, no theoretical work on electrets exhibiting bilinear dynamics. There has, however, been phenomenological treatment, most notably in the work of Perlman[9] and Gubkin,[10] of the polarization dynamics of electrets which show linear response. The experiments reported here were motivated because strong low-temperature radiation-induced-thermally-activated-depolarization (local RITAD) phenomena[11] observed recently in calcium fluoride depend very strongly on the properties of a relatively radiation-insensitive high-temperature electret state. The present experiments investigate the characteristics of this high-temperature electret, and implications regarding effects including the local RITAD phenomenon will be presented elsewhere.

The sources of electret polarization are either internal or external; external polarization is caused by the deposition or injection of charge carriers from the outside. In some systems the effects of

charge injection from electrodes are readily noticeable and manifest themselves by giving an inverted apparent final polarity of the electret. Immediately after the polarization procedure the electret surface near the positive electrode is negatively charged (i.e., positively polarized), while the surface near the negative electrode becomes positively charged. This polarization is called heterocharge polarization and is of the polarity predicted for a pure-internal-charge electret. For some electrets, particularly where very high voltages are used in the polarization procedures, the heterocharge polarization has a limited lifetime. The net electrode charge decays through zero approaching a final value having reversed polarity. The final apparent polarization at the electret surface becomes of the same polarity as the corresponding polarizing electrodes. This is called the homocharge polarization and is attributed to surface-charge-injection effects and external polarization. In the CaF_2 system we find no evidence of homocharge effects. In this paper we are concerned only with the internal polarization-heterocharge electret state of nonferroelectric materials.

Viewed microscopically there are four mechanisms which produce internal polarization in a dielectric. The first two are the ordinary electronic and ionic displacement polarizations, the third is the orientational polarization of weakly bound dipoles (sometimes referred to as dipolar polarization), and the fourth is the charge-transport polarization. Macroscopic ionic transport produces a polarization often referred to as ionic space-charge polarization.

When an externally applied electric field is suddenly changed the ordinary dielectric polarizations adjust essentially instantaneously on the time scale of our interest. The dipolar and ionic polarizations on the other hand relax to the new conditions with a finite relaxation time. A thermoelectret is one for which this relaxation time depends strongly on temperature and may range in observable values from milliseconds to years. Although not directly relevant to the thermoelectret dynamical studies described here, other physical parameters also may control electret formation rates. The most famous of these is the photoelectret effect discovered by Nadjakov[12] (1937) for which optical energy rather than thermal energy activates the electret mechanism.

The procedure for forming a stable thermoelectret is thus as follows: (i) The dielectric is placed in an external electric field at a temperature where the polarizing relaxation time is short to promote rapid attainment of equilibrium, (ii) the dielectric is then cooled, and (iii) the electric field is removed at a temperature where the relaxation time is very long. This way the polarization of the dielectric is frozen-in and electret is formed.

In ionic solids, at temperatures below about 600 °K, both the dipolar and ionic electret properties are dominated by the presence of impurity atoms or ions. Bucci and Fieschi (1966)[13,14] introduced a method, the ionic thermocurrent (ITC) method, for studying the dipolar electret states. Their original work was performed on the electret state due to the impurity-vacancy dipoles in divalent-ion-doped alkali halides. The characteristic depolarization temperature of these dipolar electrets is normally well below 0 °C. Bucci and Fieschi also found strong electret depolarization signals in their samples at high temperatures (a few hundred degrees centigrade). They attributed the dominant high-temperature depolarization signal to an ionic space-charge polarization.[15] In their samples, which were heavily doped, the space-charge electret strength appears no larger than that which we observe in relatively high-purity CaF_2. In contrast, however, to the simple thermally activated dynamic behavior we have found, the doped samples exhibit extremely complex polarization-depolarization behavior In retrospect, the complex behavior observed in heavily doped samples by Bucci and co-workers appears adequately explained by the existence of a narrow distribution of conductivity activation energies rather than the single value implied in Eq. (3).

The remaining sections describe our experimental procedures, discuss the experimental results and empirical conclusions and, finally, provide a summary of our work.

EXPERIMENTAL APPARATUS AND TECHNIQUES

The experiments reported here were performed with a metal Dewar constructed to allow electrical and optical measurements on various crystals in the temperature range from 77 °K (liquid-nitrogen temperature) to about 500 °K. To prevent the formation of frost on the crystal at low temperatures, to prevent corona discharge in high-voltage experiments, and to give appropriate thermal isolation, the crystal chamber is evacuated ($\sim 10^{-5}$ Torr) during the experiments. Most experimental work used optical-quality calcium fluoride (CaF_2: pure) in the single-crystal form, manufactured by the Harshaw Chemical Co. For comparison purposes we also used some specially doped CaF_2 crystals, manufactured by Harshaw, and some nominally pure CaF_2 crystals, manufactured by Optovac. The samples were cleaved along the (111) planes to a thickness of about 0.8 mm and a surface area of 1 cm^2.

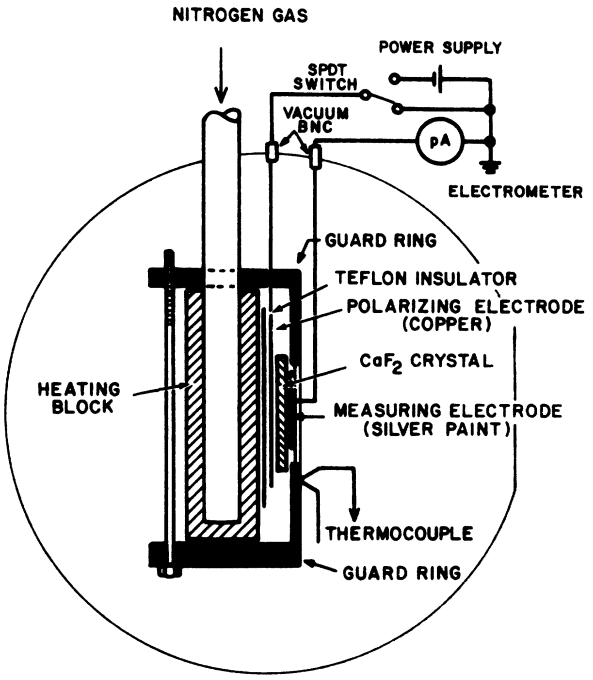

FIG. 1. Schematic representation of the heating block and the electrode arrangement.

The crystal, with an electrode placed on each side, was mounted on a hollow copper heating block. The assembly is schematically depicted in Fig. 1, which shows from left to right: heating block, a Teflon insulator, copper polarizing electrode, crystal, silver-paint measuring electrode, and guard ring. The heating block will be described later. The 75-μ-thick Teflon electrically insulates the 75-μ-thick copper electrode, which we call the polarizing electrode, from the heating block. The copper guard ring has an aperture of 0.8×0.8 cm and is in good thermal contact with the heating block. It has three important functions: First, it holds the crystal, the polarizing electrode, and the Teflon insulator in a tight contact with the heating block; second, it assures a uniform sample heating; and, third, it establishes zero potential along one surface of the crystal. The second electrode, which we call the measuring electrode, is painted on the crystal surface with a silver conductive paint to a thickness of about 15 μ. The cross section of this electrode is 0.6×0.6 cm and special care is taken to insulate it from the guard ring. Thus, both the polarizing and the measuring electrode are insulated from the system common ground and the guard ring is grounded through the heating block.

In comparison experiments, the measuring electrode may physically be separated from the sample by interposing another dielectric or by physically suspending it to produce a vacuum-gap blocking electrode. The measuring electrode is connected to ground through a picoammeter. The polarizing electrode is connected to a single-pole, double-throw (SPDT) switch and can be connected either to ground or to a polarizing voltage source, a variable dc power supply.

Separation of functions of the polarizing electrode and measuring electrode and the addition of the guard-ring structure offers considerable advantages.[16] First, it allows one to use the dc power supply and the electrometer simultaneously, with the common ground being outside of the Dewar. Second, only the sample's electret signals are sensed and those due to other insulators are not measured. The Teflon insulator, separating the polarizing electrode from the heating block, can form an electret state of its own when the polarizing electrode is connected to the power supply. But in the readout cycle this polarizing electrode is grounded and we measure only the depolarization current due to the sample's electret state from the measuring electrode. There is no depolarization current flowing on the surface of the crystal from the guard ring to the measuring electrode since they both are grounded in the polarizing cycle.

With respect to the temperature of the sample, we perform two kinds of experiments on the crystals. The first is constant-temperature studies, i.e., isothermal annealing and polarization. In the second kind of experiment, the temperature is scanned according to a known heating program. A plot of the resulting depolarization current as a function of temperature is called the depolarization *thermogram*. The most experimentally convenient heating program for these electret studies, just as for any thermally activated system's thermogram, is to heat the sample with a constant heating rate $d_t T$. In most thermally activated studies (e.g., thermoluminescence, thermally activated conductivity, etc.) an electrical heating element of some sort is placed in good thermal contact with the sample block. We, however, needed a heating scheme which would introduce minimum background-noise currents. This was achieved using the heat exchange between hot or cold nitrogen gas and a hollow copper sample block. Figure 2 shows a cut view of the inner Dewar. For crystal cooling, room-temperature nitrogen gas enters through the copper tube marked C, which is wound into a coil and emersed directly in liquid nitrogen to maximize the heat exchange between the nitrogen gas and liquid nitrogen. The cold gas then cools the sample block to liquid-nitrogen temperature (77 °K) and exits through the tube marked H in Fig. 2. For heating, the nitrogen gas first flows through a heater (not shown) built of nichrome wire wound into a coil and

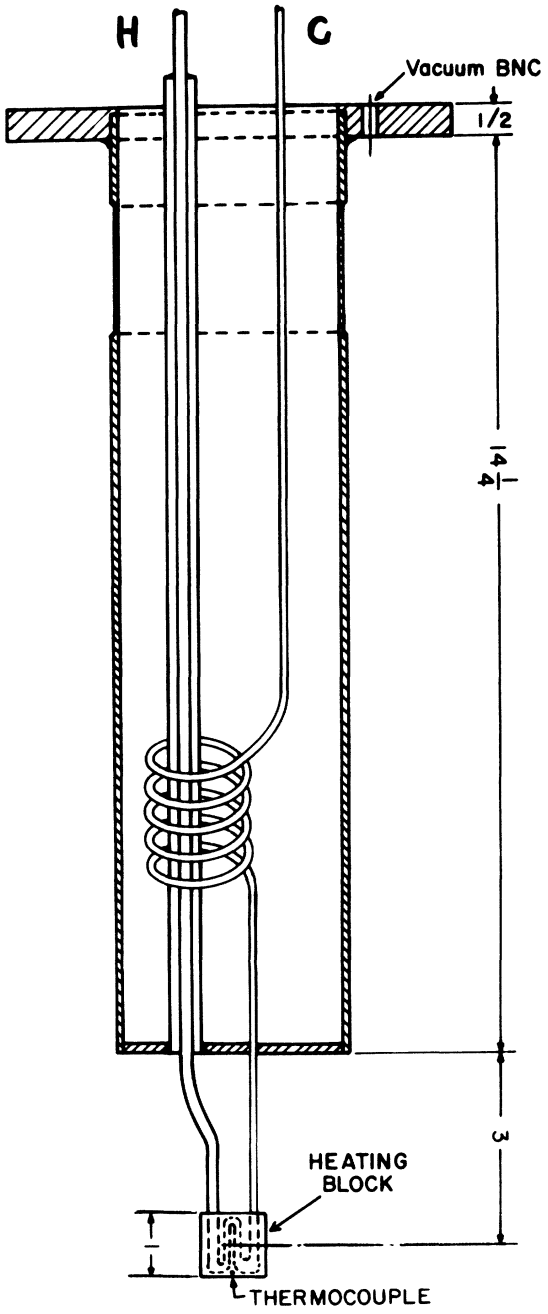

FIG. 2. Cutaway view of the inner Dewar showing the gas-flow arrangement for crystal heating and cooling (dimensions are in inches).

inserted into a Pyrex glass tube. A heater input power of 275 W heats the gas to ~ 500 °C, which is well above the temperature range of our interest. The hot nitrogen gas then passes through tube H which is surrounded by a vacuum jacket provided by a large-diameter tube. This insulates the hot input from liquid nitrogen. As long as the temperature of the heating gas is much larger than the temperature of the sample block (from 77 °K to ~ 180 °C) the sample heating is linear and reproducible. The heating rate can be varied from 0.2 to 2 °K/sec simply by regulating the nitrogen-gas flow rate through the system. The temperature was measured by a chromel-alumel thermocouple, one junction mounted on the guard ring close to the crystal and the reference junction inserted in an ice bath. Comparison experiments showed that this provides an accurate measure of the crystal temperature at least up to scan rates of 0.5 °K/sec. A digital millivoltmeter was used to measure the thermocouple emf to the nearest 10^{-2} mV, which corresponds to a temperature precision of 0.2 to 0.5 °K, depending on the position along the thermocouple calibration curve.

In isothermal experiments, the temperature is kept constant for long periods of time by a simple feedback regulation system. This opens and closes the heated nitrogen-gas flow according to whether the sample's thermocouple voltage is smaller or greater than a preset value. The temperature variations during isothermal runs were measured to be no greater than ±0.25 °K from the preset value.

EXPERIMENTAL RESULTS AND DISCUSSION

Forming an Ionic Space-Charge Electret

The effects of the ordinary electronic and ionic polarizabilities are included in the dielectric constant ϵ. Our experiments use plane parallel geometry schematically represented in Fig. 3. The electric field E in the sample is related to the total electrode charge density σ_T and the electret polarization $P(x)$ (both in esu/cm^2) by

$$E(x) = (4\pi/\epsilon)[\sigma_T - P(x)]. \quad (4)$$

Integration of Eq. (4) gives the voltage across the

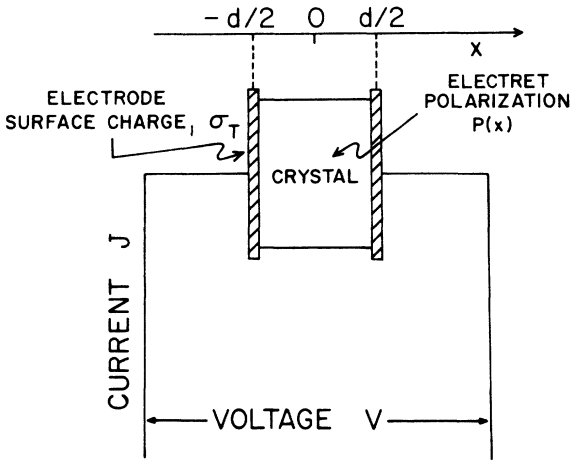

FIG. 3. Dielectric-filled parallel plate capacitor.

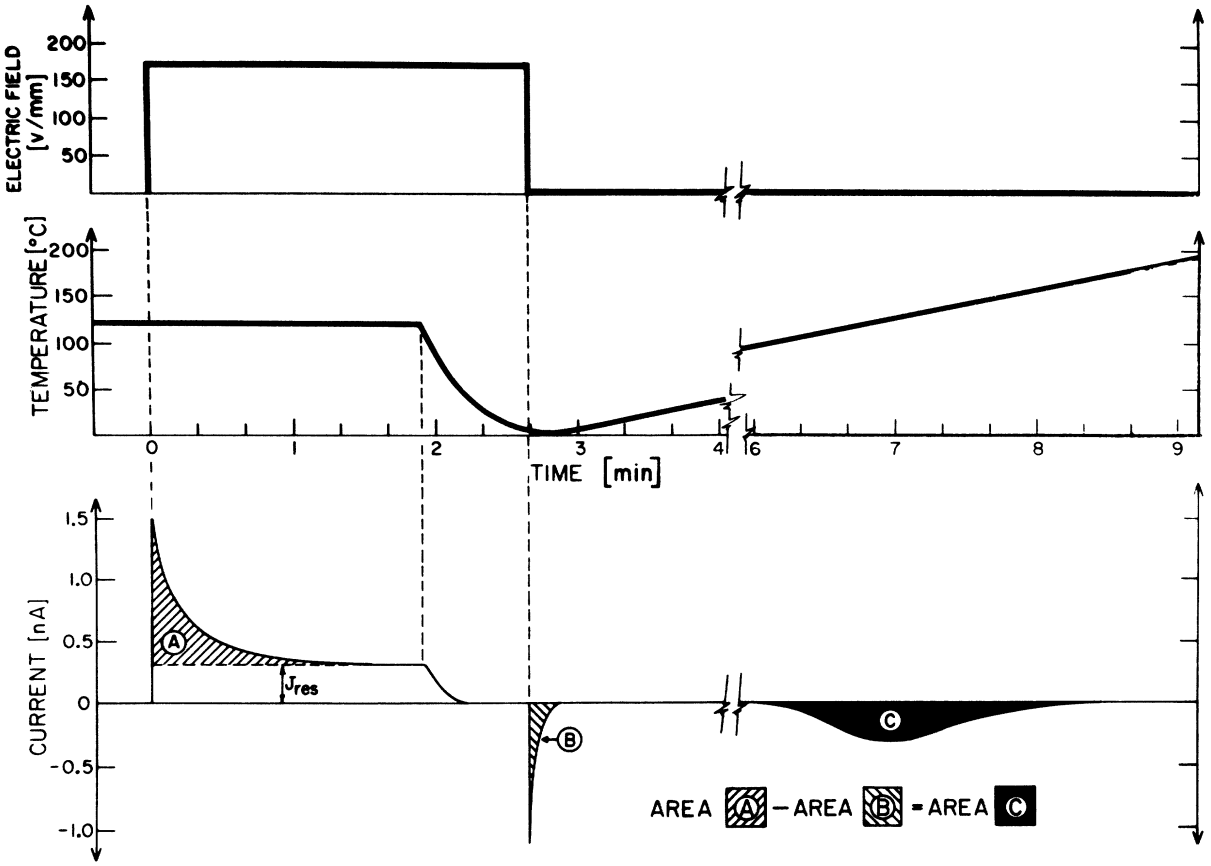

FIG. 4. Electret forming procedure: (a) electric field profile, (b) temperature profile, (c) current sensed from the measuring electrode.

sample,

$$V = (4\pi/\epsilon)[\sigma_T - \langle P\rangle]d, \tag{5}$$

where the average polarization $\langle P\rangle$ is

$$\langle P\rangle = (1/d)\int_{-d/2}^{d/2} P(x')\,dx'. \tag{6}$$

It is further convenient to write σ_T as the sum of two terms, $\sigma_V + \sigma_P$. The surface charge σ_V is required to establish the applied voltage V,

$$(4\pi/\epsilon)\sigma_V = \langle E\rangle = V/d. \tag{7}$$

The polarization electrode charge σ_P compensates the average polarization,

$$\sigma_P = \langle P\rangle. \tag{8}$$

In experiments performed with ideal blocking electrodes, no electrical charge crosses the electrode-sample interface. The current density J measured in the external circuit under constant voltage is then

$$J = \frac{d\sigma_P}{dt} = \frac{d\langle P\rangle}{dt}. \tag{9}$$

Figure 4 illustrates the electret forming procedure discussed previously. The CaF_2 crystal is held at the polarizing temperature, 125 °C for the example shown, for $t < 0$. At $t = 0$, the polarizing electrode is connected to a high-voltage dc power supply. The current flow into the measuring electrode is plotted versus time. The current decays hyperbolically to a constant value which we call the residual current J_R. The magnitude of the current depends strongly on the polarizing temperature and electric field. After the polarizing current reaches the residual value, the crystal is rapidly cooled to 0 °C and the polarizing electrode is grounded. A current spike of negative polarity is observed owing to the simple discharge of the dielectric-filled parallel plate capacitor. Area A which represents σ_T, the simple capacitor charge plus the frozen-in polarization charge σ_P, is much larger than area B representing the component σ_V. The difference is equal to the frozen-in charge σ_P, which forms the electret state. Subsequent heating of the electret with short-circuited electrodes results in a depolarization-current thermogram (area C in Fig. 4). Within our experimental accuracy of about 3%, for all electrode configurations, the charge released

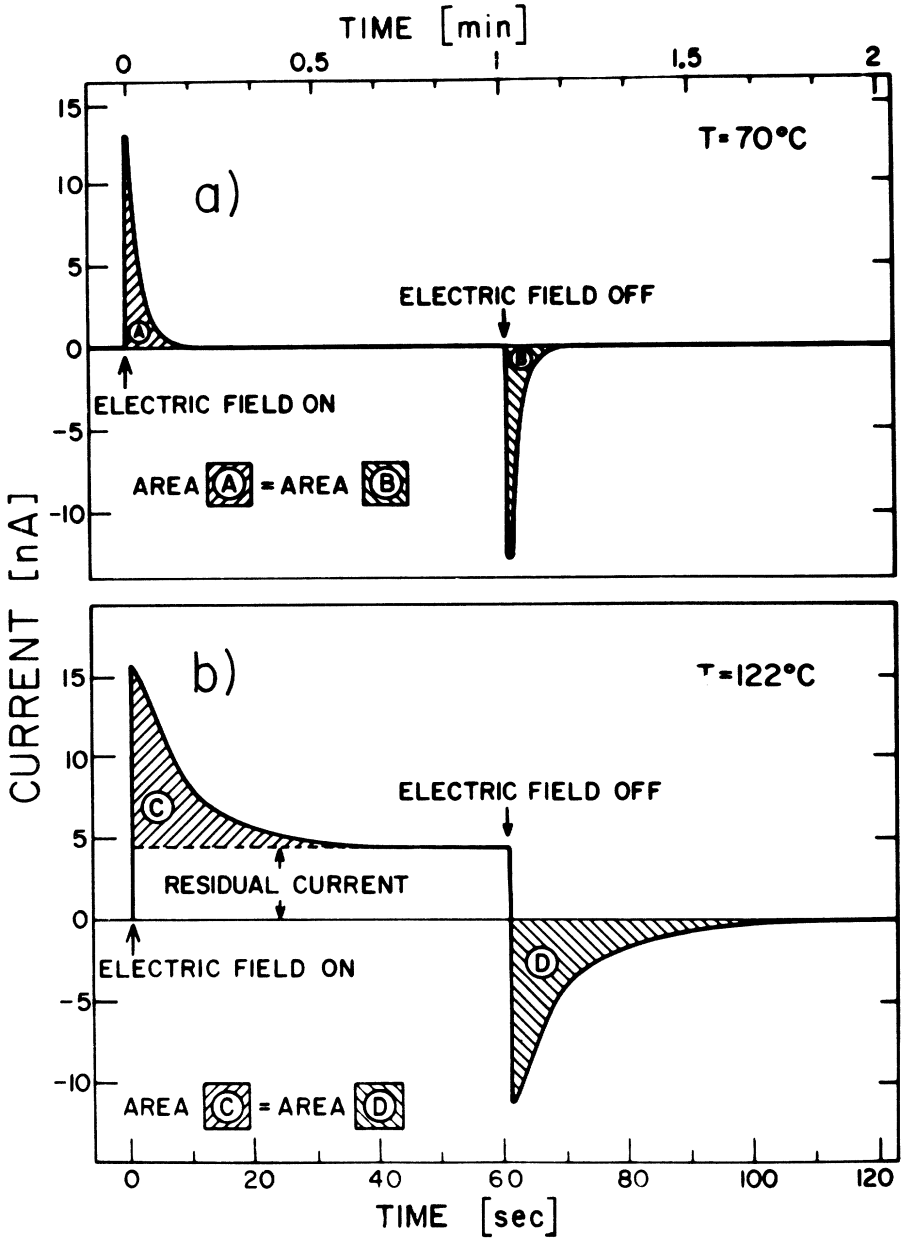

FIG. 5. Time dependence of the total polarization and depolarization current at a constant temperature. (a) $T=70\,^{\circ}\mathrm{C}$; (b) $T=122\,^{\circ}\mathrm{C}$.

under the thermogram curve is equal to the difference between the total charge σ_T and the capacitor charge σ_V. When appropriate, we can easily subtract the residual current J_R from the total current J. We can then discuss an effective surface charge σ, with

$$\frac{d\sigma}{dt} = J - J_R. \tag{10}$$

Both J and J_R are experimentally measured quantities, and J_R is zero with zero applied voltage.

In Fig. 5 we show the time dependence of the total polarization and depolarization current at a temperature of 70 °C [part (a)] and 122 °C [part (b)]. In part (a) the electret relaxation time is so long that only σ_V, i.e., the charging and discharging of the ordinary dielectric capacitor, is observed. The minimum rise time of the current pulses is a few tenths of a second and is determined by the frequency response of the recording electronics. In part (b), the electret polarization currents dominate. Three conclusions can be made on the basis of Fig. 5. First, the residual current becomes significant only at relatively high temperatures; second, the externally measured charge is conserved since (area A) = (area B) and (area C)

= (area D); and third, for a constant temperature the characteristic time for electret polarization is equal to the characteristic time for depolarization.

We have done experiments with contact electrodes where J_R is a reasonably large fraction of the initial polarizing current J, with Teflon-film insulated electrodes where J_R is a very small fraction of the initial polarizing current, and with vacuum-gap blocking electrodes where J_R is always zero. We have observed no differences among them in the dynamical behavior of σ as defined in Eq. (10). The results described above assure us that even if σ is not actually equal to σ_P, it must at least be proportional to σ_P and very nearly equal in magnitude. As the basis for discussing our results, we therefore use

$$\frac{d\sigma}{dt} = \alpha \frac{d\sigma_P}{dt} = \alpha \frac{d\langle P\rangle}{dt} , \tag{11}$$

where $\alpha \sim 1$ and is independent of other experimental variables such as the polarizing voltage or temperature.

Thermogram Results

A detailed thermogram curve shape for the ionic space-charge electret state in CaF_2 is shown in Fig. 6 (solid line) for a heating rate of 0.5 °K/sec and a crystal thickness of 0.8 mm. The initial polarizing temperature was $T_p = 125$ °C and the polarizing field $\langle E\rangle = -500$ V/mm. The total charge output was 0.05×10^{-6} C cm^{-2}. The dashed curve in Fig. 6 shows the initial rise portion of the ionic conductivity current measured as a function of temperature; the polarizing electrode is connected to the dc power supply at a voltage of the same magnitude but opposite polarity as used in polarizing the electret state. That the leading edge of the electret thermogram curve is exactly equal to the leading edge of the ionic current has been observed in all of our experimental data and suggests that the two processes are intimately related. The temperature dependence of the ionic current, $J_i(T)$, has the form

$$J_i(T) = A\, e^{-H/kT}, \tag{12}$$

where A is independent of temperature but strongly dependent on the electric field. The energy parameter H is called the activation energy. The electret depolarization current, observed in the thermogram, first increases following the ionic conductivity, but then reaches the maximum at $T_M = 402$ °K and finally drops to zero. The thermogram peak is very narrow; the full width at half-maximum is $\Delta T = \delta T_- + \delta T_+ = 32$ °K; the half-widths on the low- and high-temperature side of T_M are equal, $\delta T_- = \delta T_+$, as shown in Fig. 6. The symmetric shape of the curve suggests that a second-order process dominates the decay of the ionic space-charge electrets. The second-order, or bilinear, decay processes were first studied in thermoluminescence by Garlick and Gibson[17] (1948). A review of the bilinear decay thermograms was given elsewhere[18]; here we present only a summary of those characteristic properties pertinent to the ionic space-charge thermograms.

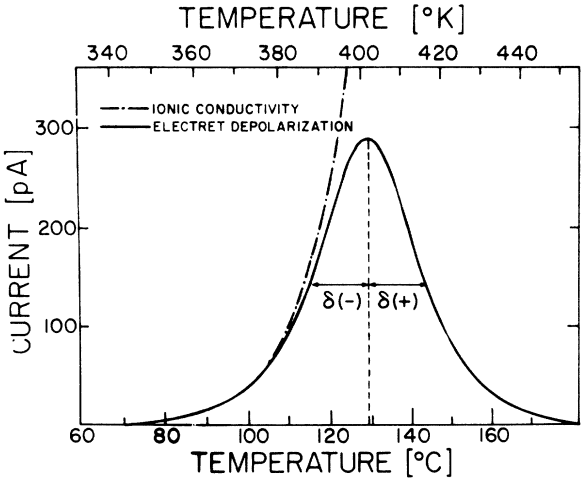

FIG. 6. The solid line shows a typical CaF_2 ionic space-charge electret thermogram and the dashed line a typical CaF_2 ionic current thermogram. The electret polarizing voltage and the ionic current applied voltage are both 500 V, but of opposite polarity. The crystal thickness was 0.8 mm; the heating rate was 0.5 °K sec^{-1}.

For strictly bilinear decay, the rate at which the electret polarization σ decays with time can be expressed in terms of the polarization and the bilinear decay constant $\gamma(T)$ given by Eq. (3),

$$\frac{d\sigma}{dt} = -\gamma(T)\sigma^2. \tag{13}$$

The first integral of Eq. (13) gives the behavior of the polarization σ as a function of time,

$$\sigma(t) = \sigma_0[1 + \sigma_0 \textstyle\int_0^t \gamma(T)\, dt']^{-1}, \tag{14}$$

where σ_0 is the initial polarization of the electret formed by applying an electric field $\langle E\rangle_P$ at temperature T_P. The discharge current J given by the thermogram is simply equal to the rate of change of polarization,

$$J(t) = -\frac{d\sigma}{dt} = \sigma_0^2\gamma(T)\left[1 + \sigma_0 \int_0^t \gamma(T)\, dt'\right]^{-2} , \tag{15}$$

which can also be written

$$J(T) = \sigma_0^2\gamma_0 e^{-H/kT}[1 + \sigma_0 \textstyle\int_0^T \gamma_0 (d_t T)^{-1} e^{-H/kT'}\, dT']^{-2} \tag{16}$$

using Eq. (3) and the heating rate $d_t T$.

Equation (16) is analogous to that derived by Garlick and Gibson for a bimolecular thermoluminescent process and, for a narrow thermogram, shows the following properties to a first-order ap-

proximation in $\Delta T/T$: (i) By setting

$$\left.\frac{dJ(T)}{dT}\right|_{T=T_M}=0,$$

a first approximation gives the following implicit relation:

$$(H/kT_M)\sim\ln[\sigma_0\gamma_0(d_tT/T_M)^{-1}]. \quad (17)$$

Equation (17) shows that the temperature of the thermogram peak T_M varies logarithmically with the initial polarization σ_0 for a bilinear decay. (ii) The thermogram curve shape is symmetrical about T_M; the half-width on the low-temperature side δT_- is equal to that on the high-temperature side δT_+. The following relation may be derived:

$$\Delta T=\delta T_-+\delta T_+\sim 3.5\,T_M(H/kT_M)^{-1}. \quad (18)$$

(iii) The peak current at T_M is approximated by

$$J(T_M)=J_M\sim\tfrac{1}{4}\sigma_0^2\gamma(T_M)$$

$$\sim\tfrac{1}{4}\sigma_0\frac{d_tT}{T_M}\frac{H}{kT_M}$$

$$\sim 0.9\,\sigma_0\frac{d_tT}{\Delta T}\,. \quad (19)$$

(iv) Regardless of any assumption about the thermogram breadth, the electret polarization σ can be written

$$\sigma(t)=\int_t^\infty J(t')dt', \quad (20)$$

and one can write the following expression for the bilinear decay rate $\gamma(T)$ using Eq. (13):

$$\left|J(t)\left[\int_t^\infty J(t')dt'\right]^{-2}\right|=\gamma(T). \quad (21)$$

To establish that the decay is indeed bilinear as given by Eq. (13), we present additional data. Figure 7 shows a semilog plot of the hyperbolic charge decay time, i.e., $|J(t)\,[\int_t^\infty J(t')dt']^{-2}|^{-1}$ versus $1/T$ as suggested by Eq. (21). We observe a $\gamma(T)$ which is, within our experimental accuracy, given by the exponential form of Eq. (3) over a three decade variation in $\gamma(T)$. The activation energy H calculated from the slope is equal to 1.32 ± 0.02 eV, while extrapolation to $(1/T)=0$ gives $\gamma_0=5\times10^{17\pm0.5}$ $\times[\mathrm{C\ sec\ cm^{-2}}]^{-1}$. We note, for future reference, that for very small remaining σ, i.e., small $1/T$ values, the data appear to show a slight trend to higher decay rates than described by Eq. (13). Using, alternatively, the approximate thermogram half-width expression of Eq. (18) we obtain $H\sim1.5$ eV; this value is in good agreement, within the approximation accuracy $\Delta T/T_M$, with that from the whole curve analysis.

Another method for the activation energy determination is the initial rise method.[17,19] It depends on the fact that when the polarization begins to decay as the temperature is raised, the integral in Eq. (16) is negligibly small and, consequently,

$$J(T)\sim\sigma_0^2\gamma_0e^{-H/kT}=\sigma_0^2\gamma(T). \quad (22)$$

The experimental results show that the description in Eq. (22) is quantitatively identical to that given by Eq. (12) for the ionic current, when σ_0 is the equilibrium polarization for the same voltage at which the ionic current is measured. Thus, the activation energies for both processes are the same. Figure 8 shows a plot of the logarithm of the current against $1/T$ for both the initial rise portion of the electret thermogram (solid line) and the ionic current (solid and dashed line). The activation energy calculated from the slope is equal to 1.30 ±0.03 eV, in good agreement with the value obtained from the full curve analysis.

Isothermal Annealing Experiments

In our isothermal decay experiments, the CaF_2 electret is polarized to equilibrium at $T_P=125\,^\circ$C. Then it is rapidly cooled to an annealing temperature T_a, where the polarizing voltage is switched to zero and the system is allowed to decay for an

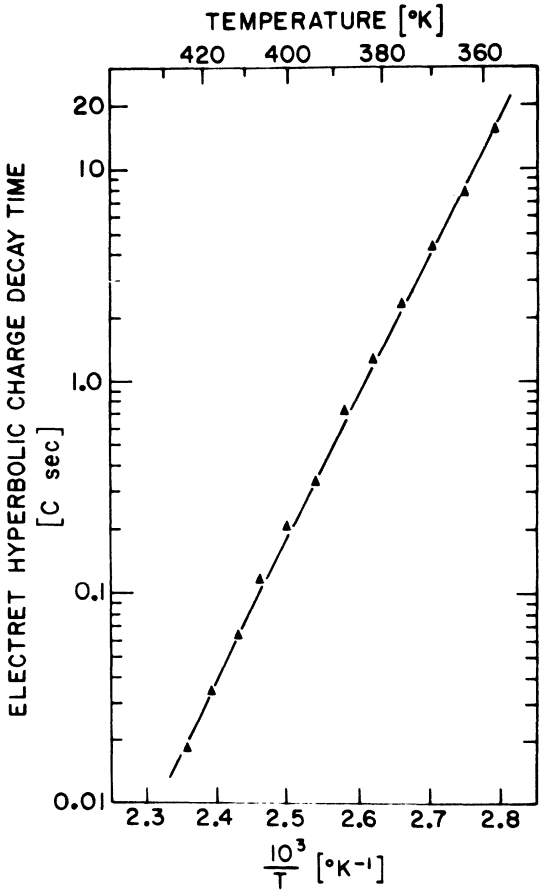

FIG. 7. Dependence of the electret hyperbolic charge decay time on temperature.

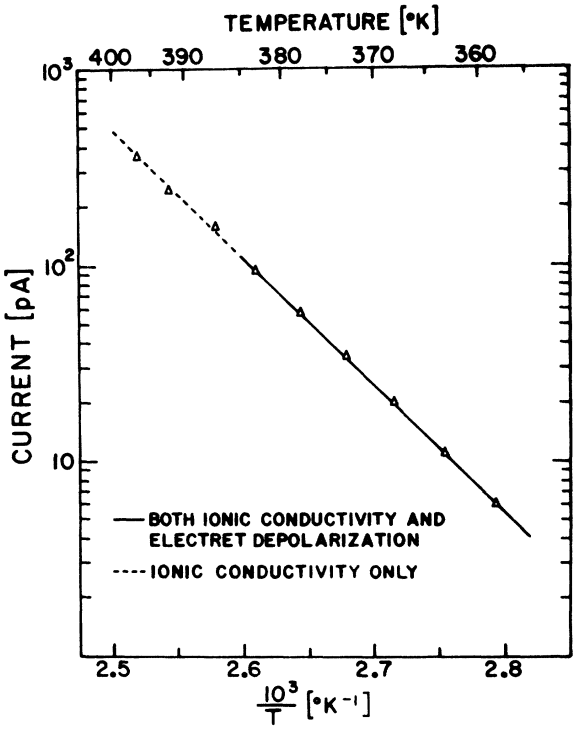

FIG. 8. Dependence of the CaF_2 ionic current (dashed and solid line) and the initial rise portion of the CaF_2 electret state (solid line) on temperature.

annealing time t_a. At the end of the annealing time a temperature scan is begun and a read-out thermogram of the remaining polarization charge is recorded. Figure 9 shows typical annealing data obtained with different annealing times for T_a = 92 °C. Equation (14) is written as follows:

$$\sigma(t)/\sigma_{eq} = [1 + \sigma_{eq}\gamma(T_a)\,t]^{-1}, \tag{23}$$

where $T = T_a$ = const, and σ_{eq} is the equilibrium polarization. The agreement between experimental points and the curve predicted by Eq. (23) is excellent; another confirmation of the bilinear decay hypothesis. Figure 10(b) shows the verification of the hyperbolic decay with a plot of $[\sigma(t)]^{-1}$ versus the annealing time. A straight line results and the electret half-life at the annealing temperature is determined. Figure 10(a) shows the dependence of the read-out thermogram peak temperature on the annealing time. From Eq. (17), the peak temperature for a bilinear process depends on the polarization σ_0, where σ_0 is a function of the annealing time. It is important to distinguish between σ_{eq}, which is the equilibrium polarization, i.e., the highest attainable polarization at a given voltage, and σ_0, which is just the polarization of the sample before the thermogram is measured. Before each annealing experiment the sample was polarized to σ_{eq} so that we can write

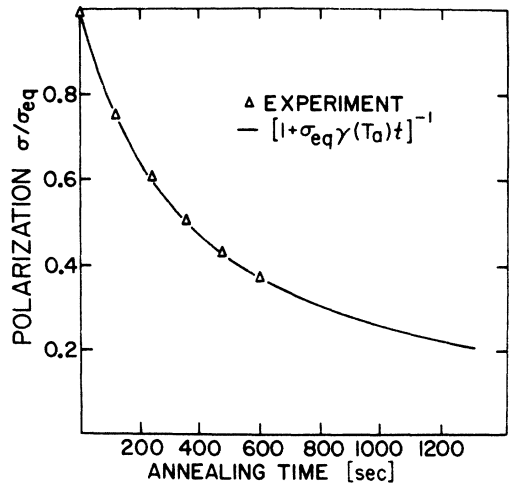

FIG. 9. Electret polarization as a function of the annealing time at an annealing temperature of 92 °C.

$$\sigma_0 = \sigma_{eq} \text{ when } t_a = 0,$$
$$\sigma_0 < \sigma_{eq} \text{ when } t_a > 0. \tag{24}$$

For a factor of 2 change in σ_0, the expression in

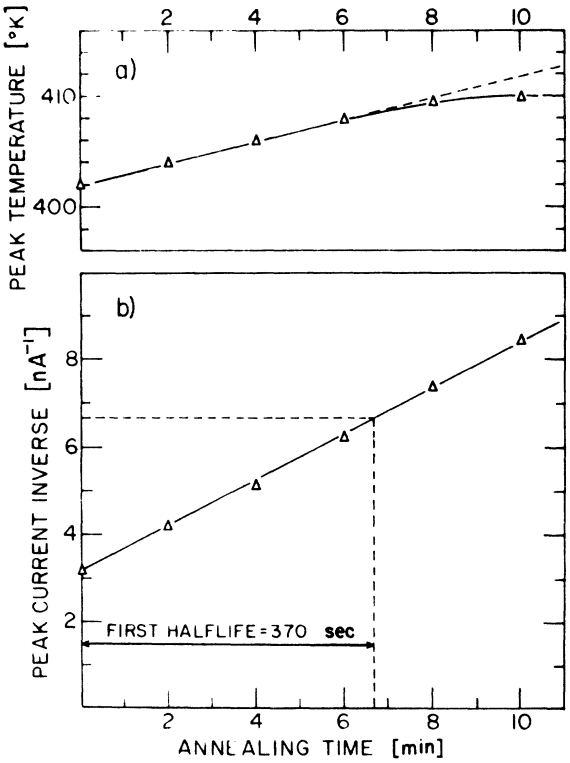

FIG. 10. (a) Dependence of the read-out thermogram peak temperature on the annealing time at an annealing temperature of 92 °C. (b) Thermogram peak current inverse as a function of the annealing time at an annealing temperature of 92 °C.

Eq. (17) predicts a shift in T_M of 7 °K for $H = 1.3$ eV and $T_M = 402$ °K. The experimental shift shown in Fig. 10(a) is 6 ± 0.5 °K in fair agreement with the predicted value.

If one attempts to follow σ to even smaller values than shown in Fig. 9, the signal-to-noise ratio becomes, of course, increasingly poor. We believe, however, that for these smaller values of σ there is a sufficient trend to indicate that T_M no longer shifts with decreasing σ and that the isothermal decay rate is larger than predicted by Eq. (13). This behavior is consistent with the very small σ behavior previously noted in the thermograms. We believe that there is, in fact, a small linear term in the actual polarization decay. Consequently, Eq. (13) is viewed as a good approximate description which is valid until linear terms begin to show their influence for $\sigma/\sigma_{eq} \ll 1$.

The isothermal hyperbolic decay half-life $t_{1/2}$ was measured for a series of annealing temperatures ranging from 50 °C ($t_{1/2} \sim 6\times10^4$ sec) to 100 °C ($t_{1/2} \sim 10^2$ sec). A semilog plot of $t_{1/2}$ versus $1/T_a$ is shown in Fig. 11. The slope of the resulting

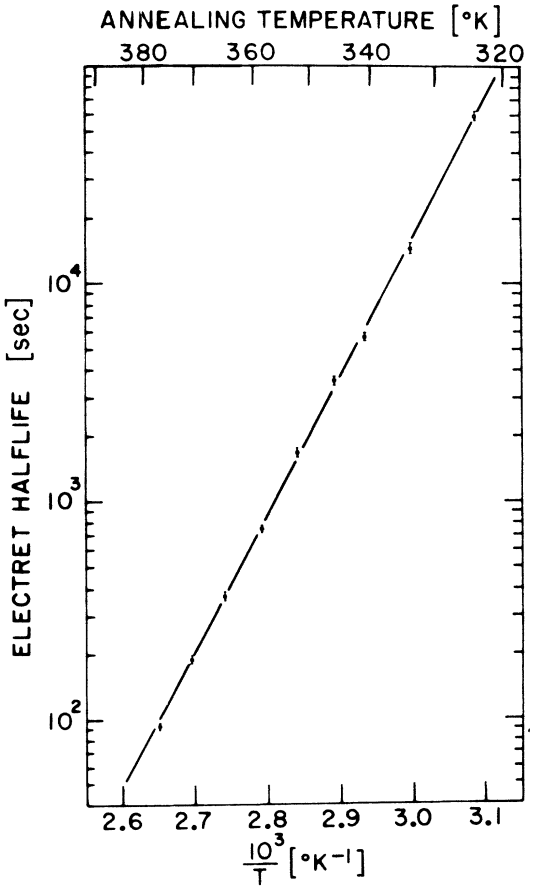

FIG. 11. CaF_2 ionic space-charge electret half-life as a function of the annealing temperature.

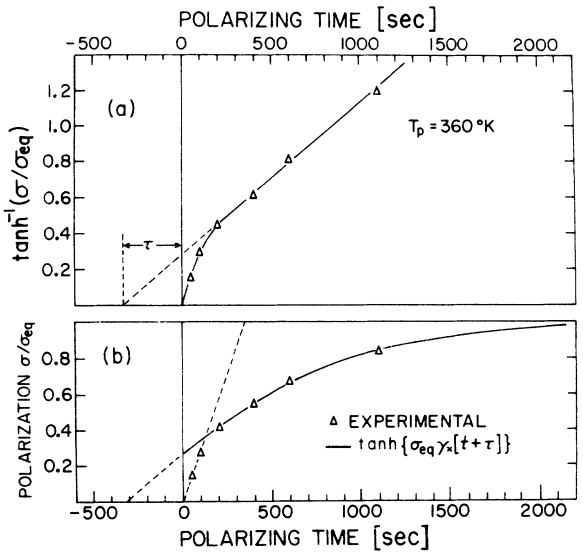

FIG. 12. CaF_2 ionic space-charge electret polarization as a function of polarizing time at a polarizing temperature of 87 °C. (a) The (inverse hyperbolic tangent) plot. (b) Hyperbolic tangent fit to σ vs t during polarization using parameters measured in previous depolarization experiments.

straight line gives the activation energy, $H = 1.28 \pm 0.02$ eV. This agrees with the values obtained at higher temperatures from the full curve analysis (1.32 eV) and from the initial rise method (1.30 eV).

The results presented so far indicate that the ionic space-charge electret depolarization is described to a high degree of approximation by the simple bilinear decay expression given by Eq. (13).

Isothermal Polarization

An initially depolarized CaF_2 crystal is held at a polarizing temperature T_p well below the thermogram peak temperature ($T_M \sim 400$ °K). At time $t = 0$, the polarizing electrode is switched to a dc power supply. The space-charge polarization grows, relaxing toward an equilibrium value, with a characteristic relaxation time which is a function of the polarizing temperature. After a polarizing time t_p, the polarizing electrode is grounded and a thermogram read-out scan is begun in order to determine the polarization $\sigma(t_p)$. Typical experimental results for isothermal relaxation to equilibrium are shown in Fig. 12(b) with $\langle E\rangle_p = 500$ V/mm, $T_p = 87$ °C, and crystal thickness $d = 0.8$ mm. Since the decay of the ionic electret state is very well described by Eq. (13), in the case of the isothermal polarization one may anticipate

$$\frac{d\sigma}{dt} = -\gamma(T)\,(\sigma^2 - \sigma_{eq}^2), \tag{25}$$

where σ_{eq} is the equilibrium polarization attained

as $t_p \to \infty$. When $V \neq 0$ then $\sigma_{eq} = 0$ and Eq. (25) reduces to Eq. (13). Integrating Eq. (25) from 0 to $\sigma(t)$ one gets

$$\sigma(t) = \sigma_{eq} \tanh[\sigma_{eq}\gamma(T_p)t], \tag{26}$$

where T_p is the polarizing temperature and t the polarizing time. Thus, according to Eq. (25), a plot of $\tanh^{-1}(\sigma/\sigma_{eq})$ versus the polarizing time should yield a straight line. Figure 12(a) shows good experimental agreement for points of relatively long polarization times, but not for points at short times. Also, the intercept of the theoretical straight line is at $t = 0$, but experimentally it is at a characteristic negative time which we denote by τ. This emphasizes a point of caution to be observed in analyzing experimental data according to Eq. (25). Suppose, for example, Eq. (25) represents a good approximation to the system's behavior, but for very small σ the real system is dominated by linear relaxation dynamics. In annealing experiments this may pass almost unnoticed because it occurs for small σ, where the signal-to-noise ratio is poor. In polarization growth experiments, however, the system begins with σ small. An initially fast linear relaxation will later be manifested as an apparent shift in the starting time of the experiment when data are analyzed according to Eq. (26). Because of the nonlinear nature of the equations, this behavior can be glaringly obvious in the polarization experiment while remaining virtually hidden in the depolarization experiment.

Consequently, the most useful solution to Eq. (25) can be expressed as

$$\sigma(t) = \sigma_{eq} \tanh[\sigma_{eq}\gamma(T)(t+\tau)], \tag{27}$$

where τ can be experimentally determined as shown in Fig. 12(a). The time τ may be roughly thought of as the time required for σ to grow to a value where Eq. (25) becomes a valid approximation. In Fig. 12(b) we plotted Eq. (27) with $\tau = 330$ sec and $\sigma_{eq}\gamma(T) = (1150 \text{ sec})^{-1}$. These values were not arbitrarily chosen for "best fit"; rather τ was experimentally determined as shown in Fig. 12(a) and $\sigma_{eq}\gamma(T)$ was calculated by extrapolation from thermogram data using Eqs. (3) and (19) with the values $d_t T = 0.6\,^{\circ}\text{K/sec}$, $\Delta T = 32\,^{\circ}\text{K}$, and $H = 1.3$ eV.

In contrast to the annealing experiments, no shifts in the read-out thermogram peak temperatures as a function of the polarizing time were observed. We cannot, at this time, offer any simple explanation. It is true, however, that the two experiments, the isothermal annealing and isothermal polarization, were not performed under identical experimental conditions. In the isothermal annealing, the sample was polarized to equilibrium at a temperature close to the thermogram peak temperature, while it was annealed at a lower temperature. In isothermal polarization, on the other hand, the sample was polarized at a temperature much lower than the thermogram peak temperature.

Equilibrium Polarization

The dependence of the equilibrium polarization on the polarizing voltage V was examined. Typical results are shown in Fig. 13 for a crystal thickness of 0.8 mm and a polarizing temperature of 125 °C. In all samples and at various polarizing temperatures the initial linear portion, $\sigma_{eq} \propto V$, was observed followed by the break into the higher-voltage behavior where $\sigma_{eq} \propto V^{1/2}$, as shown in Fig. 13.

This $V^{1/2}$ behavior has previously been observed in many materials and reported recently by Campos, Mascarenhas, and Ferreira[20] for a strong electret state in naphthalene crystals. It has been attributed[21] to Schottky barrier formation. The linear region we show in Fig. 13 occurs only at lower voltages than reported by the previous investigators. The charge release of the CaF_2 electret state polarized at 10^3 V is about a factor of 15 larger than that reported in naphthalene. The over-all σ_{eq} versus V characteristic of CaF_2 is empirically described by

$$\sigma_{eq} = 2c_e v_B^{1/2}[(V+v_B)^{1/2} - v_B^{1/2}], \tag{28}$$

where the specific capacitance is $c_e \sim 100$ pF cm^{-2} and the break point voltage is $v_B \sim 250$ V.

We also did not observe any thermogram peak temperature shifts as a function of the polarizing voltage, although one may expect a shift predicted by Eq. (17) for a second-order process. Since σ_0 varies as a function of the electric field as shown in Fig. 13, the absence of a thermogram peak tem-

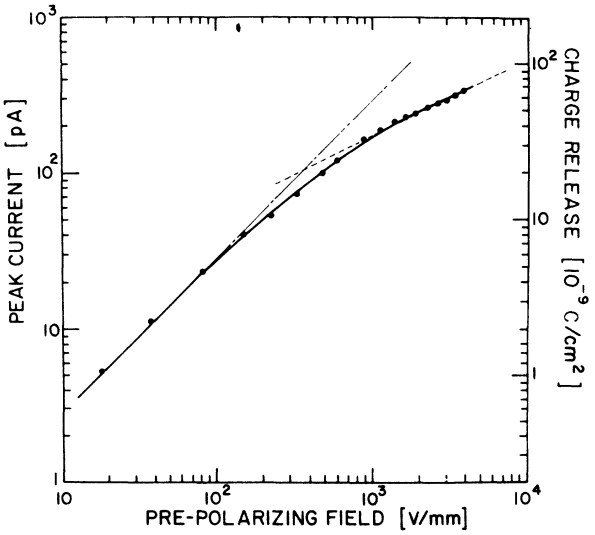

FIG. 13. Integrated equilibrium charge release and electret peak current as a function of the polarizing voltage.

perature shift can be explained only if $\sigma_0\gamma_0 = \text{const}$. We will show later that this is true atleast for relatively low electric fields.

We have attempted to study the dependence of σ_{eq} upon sample thickness and upon polarizing temperature. Both dependences are so weak that we cannot reliably measure them with the present apparatus. The equilibrium charge σ_{eq} thus depends strongly only upon the applied voltage V. Our experiments cannot rule out, however, a relatively weak temperature dependence, e.g., $\sigma_{eq} \propto 1/T$.

Ionic Conductivity

The thermally activated ionic current for unpolarized CaF_2 samples has been measured in the temperature range from 0 to about 200 °C. The observed Ohmic behavior is shown in Fig. 14 for three different temperatures and a crystal thickness of 0.8 mm. The ionic current is linear over the two-decade span in electric field accessible with our equipment. The temperature dependence of the ionic current at a given electric field was shown in Fig. 6. Figure 8 showed that the ionic conductivity is adequately described by Eq. (12), at least up to a temperature of 400 °K. We showed before that the ionic conductivity has the same activation energy as the ionic space-charge electret rate parameter $\gamma(T)$. The leading edge of the electret thermogram and of the ionic current are identical in magnitude but of opposite polarities when the applied field for ionic conductivity is equal to the polarizing field for establishing the equilibrium electret state. The initial portion, $J_0(T)$, of the electret thermogram is given by Eq. (22). When the electret is polarized to equilibrium we can write $\sigma_0 = \sigma_{eq}$ and

$$|J_0(T)| = \gamma(T)\,\sigma_{eq}^2 \,. \tag{29}$$

Equation (29) can also be written as a characteristic admitivity product multiplied by the average polarizing field $\langle E\rangle_p$,

$$|J_0(T)| = [\gamma(T)\,\sigma_{eq}^2\,\langle E\rangle_p^{-1}]\,\langle E\rangle_p \,. \tag{30}$$

Equation (12), which describes the temperature dependence of the ionic current, can also be written in the following form:

$$|J_i(T)| = [\rho(T)\,\mu(T)]\,\langle E\rangle, \tag{31}$$

where ρ is the mobile charge density, $\mu(T)$ the thermally activated mobility, and $\langle E\rangle$ is the applied field. Comparing Eq. (30) with Eq. (31) the experimental result implies the following expression for the decay rate $\gamma(T)$:

$$\gamma(T) = [\rho(T)\,\mu(T)\sigma_{eq}^{-2}]\,\langle E\rangle \,. \tag{32}$$

We showed in Fig. 13 that there are two different regions in the functional dependence of σ_{eq} on the polarizing field $\langle E\rangle_p$, namely, the low-field linear region ($\sigma_{eq} \propto \langle E\rangle_p$) and the high-field equadratic region ($\sigma_{eq}^2 \propto \langle E\rangle_p$). From Eq. (32) we see that in the linear region $\gamma(T)$ is inversely proportional to $\langle E\rangle_p$. This behavior may explain the absence of thermogram peak temperature shifts when we vary $\sigma_0 = \sigma_{eq}$ by varying the polarizing voltage. That is, the T_M shift predicted in Eq. (17) depends upon the product $\sigma_0\gamma_0$. In the polarization experiments, $\sigma_0 = \sigma_{eq} \propto V$, while $\gamma_0 \propto V^{-1}$ and the product $\sigma_0\gamma_0$ is a constant. Thus T_M remains constant as σ_{eq} is varied. On the other hand, in the depolarization experiments, we varied σ_0 by annealing the samples, which were always polarized with the same voltage and at much higher temperature. Consequently, in depolarization, γ_0 does not vary as σ_0 varies, so the product $\sigma_0\gamma_0$ is not a constant and a shift in T_M is observed.

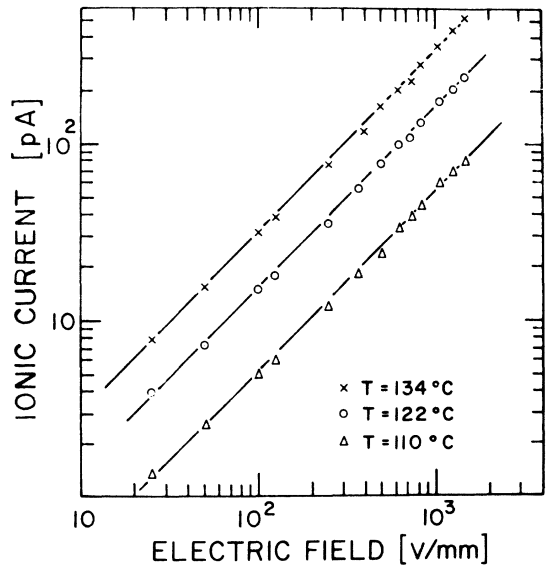

FIG. 14. Ionic current as a function of the applied electric field at various temperatures. (Crystal thickness 0.8 mm.)

Other Samples

Even in these high-purity CaF_2 samples, there remain trace concentrations of trivalent impurity ions which are charge compensated locally by fluorine-ion interstitials. At low temperatures this complex remains bound to form a local dipolar state. The first-order kinetics of the resulting low-temperature weak dipolar electret has been studied extensively by Mascarenhas and coworkers.[22,23] We also obtained a CaF_2 sample doped to 0.1 at.% with europium from Harshaw Chemical Co., and measured the dipolar electret strength by performing low-temperature ionic-thermocurrent (ITC) depolarization experiments. We could then compare against ITC signals in our

high-purity samples. The results are shown in Fig. 15 for a polarizing field of 10^3 V/mm. In the CaF_2:Eu, we find detailed agreement with the results of previous investigators for the thermal reorientation of the (trivalent-ion–fluorine-interstitial) dipolar complex. The CaF_2:Eu dipolar thermogram can readily be analyzed. It is asymmetric with the ratio of half-widths, $\delta T_-/\delta T_+$, approximately equal to 1.5, which characterizes a linear decay mechanism. The peaking temperature T_M is ~148 °K, while the full half-width is $\Delta T = \delta T_- + \delta T_+ \sim 10$ °K. An approximate expression[18] for a first-order process is $\Delta T \sim 2.44\, T_M (H/kT_M)^{-1}$. From this we estimate the activation energy of 0.46 eV for the dipolar reorientation. In our high-purity samples, the ITC signal is about a factor of 10^2 weaker, corresponding to a trivalent-ion impurity concentration of approximately 10 ppm.

It was found by Ure (1957)[24] that the principal defect in CaF_2 is the anti-Frenkel disorder,[25] i.e., F^- vacancies and interstitials. In the high-temperature regime, the compensating negative ions tend to dissociate from the trivalent ions. It has been presumed that their mobility dominates the nonintrinsic low-temperature tails of the sample's ionic conductivity. In comparison experiments, however, we find that the CaF_2:pure and CaF_2:Eu samples manufactured by Harshaw show essentially identical ionic conductivity and essentially identical space-charge electret behavior.

In contrast, we obtained a sample of nominally pure Optovac CaF_2, and found it to have a factor of 10^2 greater ionic conductivity than either one of the Harshaw samples. The space-charge electret thermograms of the Optovac sample show a T_M shifted to 20 °K lower temperature than for the Harshaw material. This shift is just equal to that predicted from the previous observation that $\gamma(T)$ scales as the ionic conductivity. We were, however, surprised to find apparently no appreciable differences in the σ_{eq} versus V characteristics for the Harshaw and Optovac samples. Low-temperature ITC studies of the Optovac samples show, on the other hand, a small signal comparable to that measured in the Harshaw high-purity samples.

We suspect that, because Eu^{3+} has only a small atomic binding energy for the third "hole," it can easily convert to Eu^{2+} by stealing the compensating ion's electron. Consequently, the high-temperature dissociation of the $Eu^{3+}F^-$ complex may yield Eu^{2+} and F^0, which will contribute neither to ionic conductivity nor to the space-charge electret state.

SUMMARY

The space-charge electret state observed in CaF_2 at a depolarization temperature around 400 °K has a short-circuit polarization decay very well described by a simple second-order kinetics equation, $d_t\sigma = \gamma(T)\,\sigma^2$. By combining isothermal decay and thermogram experiments we can follow $\gamma(T)$ over about a five-decade variation. We find that $\gamma(T)$ is a simple thermally activated function $\gamma(T) = \gamma_0 e^{-H/kT}$ with the activation energy $H = 1.30 \pm 0.02$ eV. Moreover, $\gamma(T)$ is directly proportional to the material's bulk ionic conductivity.

Isothermal polarization studies show that the electret formation mechanism is also governed by bilinear dynamics having the same rate parameter $\gamma(T)$; $d\sigma/dt = -\gamma(T)[\sigma^2 - \sigma_{eq}^2]$. Experimental results are well approximated by the solution $\sigma(t) = \sigma_{eq}\tanh[\sigma_{eq}\gamma(T)(t+\tau)]$. The observation of a finite value for τ implies that the real electret system has some small linear relaxation terms which dominate for $\sigma/\sigma_{eq} \ll 1$.

The equilibrium electret polarization σ_{eq} first rises linearly with polarizing voltage and then for voltages greater than about 10^3 V follows a $V^{1/2}$ dependence. The electret strength σ_{eq} is very large; we attain polarizations of about 0.05×10^{-6} C cm^{-2} for a 1-kV applied potential. In every case

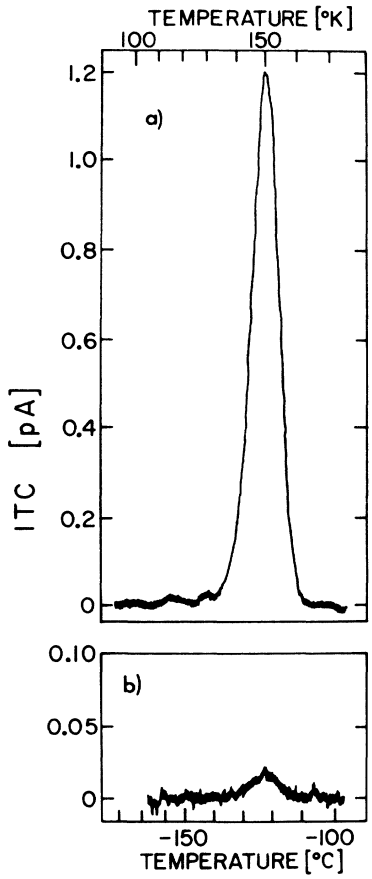

FIG. 15. Weak dipolar electret state (ITC) in CaF_2 with a polarizing field of 10^3 V/mm and crystal thickness of 0.8 mm. (a) Eu-doped crystal; (b) nominally pure crystal.

the product $\sigma_{eq}^2 \gamma(T) \langle E \rangle^{-1}$ is equal, by direct comparison, to the measured ionic conductivity. The preexponential factor γ_0 appears to be inversely proportional to the polarizing voltage in the linear [σ_{eq} versus V] region.

The above results establish that a single mechanism governs the entire electret polarization-depolarization process. In this case, that mechanism is the charge transport due to ionic conduction. The bilinear dynamics and the breakover of σ_{eq} into a $V^{1/2}$ dependence lead us to suspect that the formation of Schottky ionic depletion regions may be involved. In no case have we ever observed homocharge formation as often seen in other strong electret systems.

We can compare our results with previous experiments on space-charge electret states in ionic solids. We observe an extremely narrow depolarization thermogram whose half-width is characteristically about 8% of its peak temperature. Experiments previously reported for other space-charge electrets show an almost hopelessly complex polarization-depolarization behavior. The thermogram maximum T_M shows large increasing shifts with increasing polarization temperature, the polarization charge is nonlinear in applied polarizing voltage for low voltages, the thermogram half-width is more than a factor of 3 larger than that we observe, and the thermogram has much more severely truncated wings than the thermogram shapes we observe. Such complexity has largely discouraged further experimentation or attempts at interpretation of results.

We feel encouraged, however, that most of this complexity observed in other systems can be at least qualitatively predicted by the following model. Suppose that the impurity doping is not well controlled so that, rather than the single activation energy implied by Eq. (3), there is a small spread in activation energies. The electret behavior would then reflect the dynamics of a multicomponent system. While each component behaves according to Eq. (3) the composite electret state shows exceedingly complicated behavior corresponding qualitatively to the previous experimental observations.

We have also found that, although the ionic conductivity and $\gamma(T)$ vary strongly with trace impurity content of samples from different sources, the equilibrium polarization value $\sigma_{eq}(V)$ does not.

We feel, therefore, that the strong space-charge electret properties of ionic solids are a simple consequence of ionic conductivity charge transport. In samples of controlled impurity content, the resulting dynamical behavior can be very simply described empirically. We hope that this simplicity will recommend itself to theoretical efforts in interpreting how the ionic charge transport actually produces the observed effects.

ACKNOWLEDGMENTS

The authors thank Gene Fuller, Professor Sergio Mascarenhas, and David Pearson for helpful discussions during the course of the experiments. We also thank John Thompson for help in building the apparatus and Orlando Canto, who prepared all of the figures. A contract with the U. S. AEC supported the initial phases of this program relating to radiation dosimetry. Basic reasearch on the detailed dynamics of the electret state was supported by NSF (Division of Materials Research).

---

†Work supported in part by the U. S. Atomic Energy Commission (Contracts Division) and the National Science Foundation (Division of Materials Research).

[1]B. Gross, Endeavour XXX, No. 111 (1971).
[2]M. M. Perlman, in *Electrets and Related Charge Storage Phenomena* (The Electrochemical Society, New York, 1968), p. 3.
[3]B. Gross, J. Appl. Phys. **43**, 2449 (1972).
[4]S. Mascarenhas, Indian J. Pure Appl. Phys. (to be published).
[5]M. Eguchi, Philos. Mag. **49**, 179 (1925).
[6]B. Gross, in *Charge Storage in Solid Dielectrics* (Elsevier, Amsterdam, 1964).
[7]*Electrets and Related Charge Storage Phenomena*, edited by L. Baxt and M. M. Perlman (The Electrochemical Society, New York 1968).
[8]Proceedings of the 142nd Meeting of the Electrochemical Society, Miami Beach, Fla., 1972 (unpublished).
[9]M. M. Perlman, Electrochem. Technol. **6**, 95 (1968).
[10]V. M. Fridkin and I. S. Zheludev, in *Photoelectrets and the Electrophotographic Process* (Consultants Bureau, New York, 1960).
[11]E. B. Podgoršak and P. R. Moran, Science **179**, 380 (1973).
[12]G. Nadjakov, C.R. (Dokl.) Acad. Sci. URSS **204**, 1865 (1937).
[13]C. Bucci and R. Fieschi, Phys. Rev. Lett. **12**, 16 (1964).
[14]C. Bucci, R. Fieschi, and G. Guidi, Phys. Rev. **148**, 816 (1966).
[15]C. Bucci and S. C. Riva, J. Phys. Chem. Solids **26**, 363 (1965).
[16]The authors are indebted to Professor S. Mascarenhas who pointed out these advantages to them.
[17]G. F. J. Garlick and A. F. Gibson, Proc. R. Soc. A **60**, 574 (1948).
[18]P. R. Moran and E. B. Podgoršak, U. S. Atomic Energy Commission Progress Report No. C00-1105-164, 1971 (unpublished).
[19]C. Haake, J. Opt. Soc. Am. **47**, 649 (1957).
[20]M. Campos, S. Mascarenhas, and G. L. Ferreira, Phys. Rev. Lett. **27**, 1432 (1971).
[21]H. K. Henish, in *Rectifying Semiconductor Contacts* (Oxford U. P., New York, 1957), p. 214.
[22]J. Wagner and S. Mascarenhas, Phys. Rev. Lett. **27**, 1514 (1971).
[23]B. S. H. Royce and S. Mascarenhas, Phys. Rev. Lett. **24**, 98 (1970).
[24]R. W. Ure, J. Chem. Phys. **26**, 1363 (1957).
[25]W. Bollman, P. Gorlich, W. Hauk, and H. Mothers, Phys. Status Solidi A **2**, 157 (1970).